Eur. Phys. J. D **19**, 403–410 (2002)
DOI: 10.1140/epjd/e20020088

THE EUROPEAN PHYSICAL JOURNAL D
EDP Sciences

Control of the pulse duration in one- and two-axis passively Q-switched solid-state lasers

N.D. Lai[a], M. Brunel, F. Bretenaker, and O. Emile

Laboratoire d'Électronique Quantique-Physique des Lasers[b], Université de Rennes I, Campus de Beaulieu, 35042 Rennes Cedex, France

Received 3 December 2001

Abstract. We study theoretically and experimentally different methods to control the pulses emitted by solid-state lasers passively Q-switched by a saturable absorber. We explore one- and two-axis laser schemes allowing to control the pulse duration, which is ruled by the saturation powers of the transitions in the absorber and in the gain medium. In one-axis lasers, it is shown that the adjustment of the pump and laser beam sizes in the active medium and in the absorber provides an efficient means to control the pulse temporal shape and duration. Furthermore, a two-axis laser cavity supporting so-called forked-eigenstate operation permits to freely adjust the parts of the mode power which circulate in the gain medium and in the absorber. In this case, a lengthening of the pulse duration up to 500 ns is obtained with an increase of the average output power. The theoretical results obtained by using rate equations adapted to each cavity geometry are in close agreement with experiments performed on a diode-pumped Nd^{3+}:YAG laser Q-switched by a Cr^{4+}:YAG saturable absorber. The relevance of the different techniques to control the pulse durations in the framework of potential applications is discussed.

PACS. 42.55.Ah General laser theory – 42.60.Gd Q-switching – 42.55.Rz Doped-insulator lasers and other solid state lasers

1 Introduction

Diode-pumped solid-state lasers passively Q-switched by saturable absorbers are compact and rugged sources of pulsed radiation suited to a wide range of applications [1–7]. The main characteristics of the emitted pulses are their duration, peak power, and repetition rate. While the latter is adjustable simply by choosing the pump power, the pulse duration and peak power are known to be ruled by the parameters of the gain medium, the absorber, and the cavity [8]. They are thus essentially fixed by laser construction. For applications requesting the control and adjustment of the pulse temporal shape, such as, *e.g.*, range finders, only active systems have yet been studied [9,10]. However, theoretical descriptions of passively Q-switched lasers show that the pulse duration and shape rely on the ratio R of the saturation power in the gain medium to the saturation power in the absorber [8, 11–13]. One can hence wonder how to introduce an extra degree of freedom in the laser which would allow a continuous control of the parameter R, and consequently of the shape of the pulses. The first path one can follow consists in questioning how the pulse duration can be affected by the pump and laser mode sizes. On the one hand, the relative internal laser mode sizes in the gain medium and in the absorber can be varied. On the other hand, the external pump mode size can be changed in the gain medium, as suggested by a recent theoretical study [13]. Besides, a technique permitting to change artificially the ratio R can be explored, when two-axis lasers oscillating on forked eigenstates are considered [14,15]. Indeed, in this case, the electromagnetic field experiences a spatial separation in one part of the cavity. One may hence question the possibilities of such a scheme to control the powers circulating in the gain medium and in the absorber.

To address these different points, we choose the following plan. In Section 2, we first explore a theoretical model based on rate-equations of a single-axis laser to study the effect of the variations of R on the pulse duration. The predictions of the model are then compared with experiments made with a Nd:YAG laser passively Q-switched by a Cr:YAG saturable absorber. In order to isolate the roles played by the active medium and absorber saturation powers, we use two different cavity geometries. On the one hand, we vary the ratio w_A/w_G of the laser mode radius in the saturable absorber to the laser mode radius in the gain medium. On the other hand, we vary the ratio w_P/w_G of the pump mode to laser mode radii inside the gain medium. In Section 3, we extend the rate-equation model to the case of a two-axis laser containing a double-refraction crystal and a quarter-wave plate. The predictions are then tested experimentally on a two-axis

[a] e-mail: lai.ngocdiep@univ-rennes1.fr
[b] UMR 6627 du CNRS

laser cavity supporting forked-eigenstate operation with the gain and absorber media placed in separate arms of the cavity. Finally, the experimental results obtained using the different scenarios to control the pulse duration are summarized and compared in Section 4. The possibilities offered by these methods as regards to applications are discussed.

2 Single axis laser: control by the mode sizes

Let us first consider the laser depicted in Figure 1a. The resonator has a length L and is closed by two mirrors M_1 and M_2. It contains an isotropic solid-state active medium and a saturable absorber. It is longitudinally pumped by a cw laser diode. When the pumping yields enough population inversion in the gain medium to overcome the unsaturated losses (first threshold), the photon number grows at a rate which depends not only on the photon round-trip time but also on the rate at which the absorber and the gain medium saturate. Indeed, if the saturable absorber is fully bleached before the gain reaches its saturated value (the so-called "second threshold" condition [8]), a giant pulse is emitted. This well-known behavior may be modeled by a set of scalar rate-equations for three variables: the intracavity power, the upper level population of the laser transition and the absorption in the saturable absorber [16]. In order to match the experimental conditions presented in the following, we add to these usual variables the lower level of the laser transition, which happens to have a finite lifetime [17,18]. We also take into account the absorption of the saturable absorber in its excited-state [19–21]. Finally, the laser is assumed to oscillate in one linearly polarized eigenstate only. Consequently, the laser behavior is governed by the following differential equations:

$$\frac{\mathrm{d}I}{\mathrm{d}t} = -\left[\Gamma + a + (a_0 - a)\frac{\sigma_{\mathrm{ESA}}}{\sigma_{\mathrm{GSA}}}\right] I + \kappa(n_{\mathrm{u}} - n_{\mathrm{d}})I + \kappa n_{\mathrm{u}}\varepsilon, \tag{1a}$$

$$\frac{\mathrm{d}n_{\mathrm{u}}}{\mathrm{d}t} = \gamma_{\mathrm{u}}(P - n_{\mathrm{u}}) - \zeta(n_{\mathrm{u}} - n_{\mathrm{d}})I - \zeta n_{\mathrm{u}}\varepsilon, \tag{1b}$$

$$\frac{\mathrm{d}n_{\mathrm{d}}}{\mathrm{d}t} = \gamma_{\mathrm{u}} n_{\mathrm{u}} - \gamma_{\mathrm{d}} n_{\mathrm{d}} + \zeta(n_{\mathrm{u}} - n_{\mathrm{d}})I + \zeta n_{\mathrm{u}}\varepsilon, \tag{1c}$$

$$\frac{\mathrm{d}a}{\mathrm{d}t} = \gamma_{\mathrm{a}}(a_0 - a) - \mu a I, \tag{1d}$$

where I is the intracavity laser power, n_{u} and n_{d} are the populations of the upper and lower levels of the laser transition, respectively, a is the saturable absorption, Γ is the cavity decay rate, κ and ζ are ion/field coupling coefficients in the active medium, ε is a small heuristic term which holds for the spontaneous emission, γ_{u} and γ_{d} are the relaxation rates of the upper and lower laser levels, respectively, P is the pumping rate normalized to the upper level decay rate, γ_{a} is the relaxation rate of the saturable absorption, a_0 is the small-signal (unsaturated) absorption, σ_{GSA} and σ_{ESA} are the ground-state and excited-state absorption cross-sections of the saturable absorber,

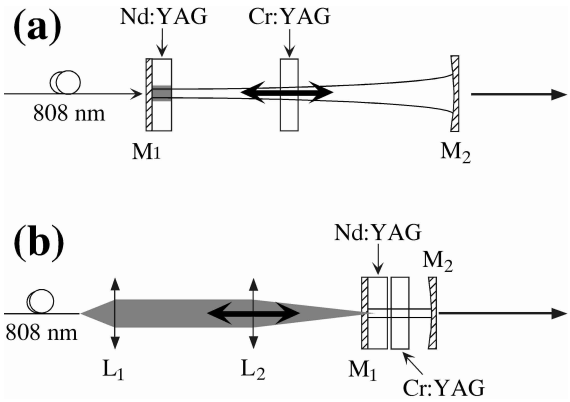

Fig. 1. Experimental arrangement of the one-axis laser: Nd:YAG, active medium; Cr:YAG, saturable absorber; L_1, L_2, focusing lenses; M_1, plane mirror; M_2, concave mirror. (a) Translation of the absorber; (b) translation of the focusing lens.

respectively. The ratio R of the saturation power in the gain medium to the saturation power in the absorber is related to the ion/field coupling coefficients μ and ζ in the saturable absorber and in the gain medium, respectively, by:

$$R = \frac{\gamma_{\mathrm{u}}}{\gamma_{\mathrm{a}}}\frac{\mu}{\zeta}\cdot \tag{2}$$

In the following, we investigate the Q-switching mechanism when R is varied. With the parameters given by the experiments as specified below, and with the following parameters which are common to all the experiments: $\sigma_{\mathrm{ESA}}/\sigma_{\mathrm{GSA}} = 0.27$, $1/\gamma_{\mathrm{u}} = 230$ μs, $1/\gamma_{\mathrm{d}} = 10$ ns, $\kappa = \zeta = 1$, $1/\gamma_{\mathrm{a}} = 4$ μs, $\varepsilon = 10^{-20}$, the laser behavior is obtained by a numerical integration of equations (1) using a fourth-order Runge-Kutta algorithm [22].

2.1 Translation of the absorber

We first choose to change the ratio R by varying the beam section area in the absorber while keeping the beam waist in the gain medium unchanged. Experimentally, this is obtained simply by translating the absorber along the propagation axis of the laser cavity, as depicted in Figure 1a. M_1 is highly transmitting ($T_1 > 95\%$) at 808 nm and highly reflecting ($R_1 > 99.5\%$) at 1 064 nm. It is directly coated on the active medium which is a 1.1 mm long crystal of 1 at.% doped Nd:YAG. The output coupler M_2 (transmission $T_2 = 1\%$ at 1 064 nm) is a spherical mirror of 100 mm radius of curvature. The saturable absorber is a 1 mm long antireflection coated Cr^{4+}:YAG plate. It is [100]-cut and its small-signal power transmission at 1 064 nm is 90%. For this case, the laser is pumped by a 800 mW fiber-coupled laser diode emitting at 808 nm. The end of the fiber is simply butted against the Nd:YAG crystal. The cavity length is chosen equal to 90 mm in order to be able to move the saturable absorber inside the cavity. Owing to this cavity geometry, the laser beam radius increases from 100 μm at its waist on mirror M_1

Table 1. Laser parameters used for simulations in the three cases corresponding to cavities depicted in Figures 1a, 1b, and 4.

Parameters	Units	Figure 1a	Figure 1b	Figure 4
Γ	s^{-1}	5.0×10^7	28.5×10^7	5.0×10^7
a_0	s^{-1}	3.5×10^8	18.1×10^8	3.5×10^8
ϕ	(°)	n/a	n/a	5.7
R		varies	varies	0.05
ρ	(°)	n/a	n/a	varies

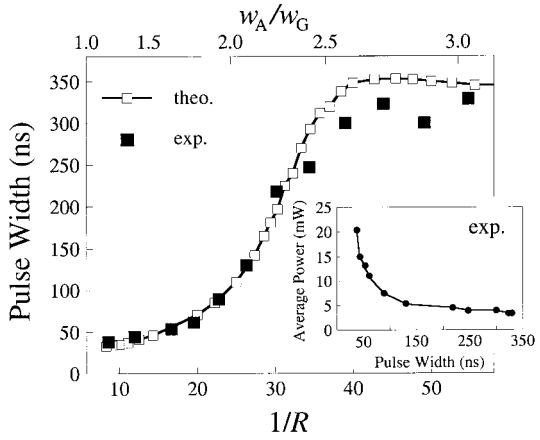

Fig. 2. Pulse width *versus* $1/R$ and w_A/w_G obtained by translation of the absorber. Open squares: simulation results; filled squares: experimental result. The horizontal scales are related by $1/R = 3.46(w_A/w_G)^2$. Inset: measured average output power *versus* pulse width.

to 320 μm on mirror M_2. When the Cr^{4+}:YAG plate is placed against the active medium, this laser emits a train of Q-switched pulses of 38 ns full-width at half-maximum at a 11 kHz repetition rate. It oscillates in a single longitudinal mode and its average output power is measured to be 20 mW. Using the experimental parameters (given in Tab. 1) and with $R = 0.12$, the computation of the differential equations yields a train of Q-switched pulses emitted at a repetition rate of 10 kHz with a pulse width of 33 ns, close to the experimental value. We further explore the variations of the pulse parameters as the ratio R is varied. If now R decreases, the relative intensity in the absorber is expected to decrease. As a result, the stimulated emission process is slowed and the pulse width increases. It is hence expected that lower values of R lead to longer pulses (slow Q-switching regime). Indeed, when R is varied from 0.12 to 0.018, the simulation yields pulse widths increasing from 33 ns to 350 ns, as shown in Figure 2. Moreover, we obtain theoretical repetition rates ranging from 10 kHz to 71.5 kHz.

As the ratio R corresponds to the ratio of saturation powers in the gain medium and in the absorber, it should be proportional to the square of the beam section area. To check this prediction, we change experimentally the beam section area in the saturable absorber by translating the Cr^{4+}:YAG plate along the laser axis, while keeping the beam waist in the gain medium unchanged. We then observe that the pulse duration is increased by a factor of 8.7 while the ratio w_A/w_G increases by a factor of 2.7. This is also shown in Figure 2 to compare with the simulations. As shown in this figure, the pulse width is stretched from 38 ns to 350 ns, in agreement with the theoretical results. The relation $1/R = 3.46(w_A/w_G)^2$ is found to lead to a good agreement between the experimental and theoretical results. The experimental repetition rates range from 11 kHz to 71 kHz, also in good agreement with the model. Finally, we find both theoretically and experimentally that the average output power decreases monotonously when the pulse width increases, as shown in the inset of Figure 2.

Using this usual laser cavity set-up, it is demonstrated that the pulse duration can be changed by varying w_A/w_G. This is reproduced by the rate-equations model simply by a variation of the ratio R. But, in cases where the mode radius is almost constant in the laser cavity, as in microchip lasers for instance, this internal degree of freedom used above disappears. However, an external degree of freedom may be found. Indeed, by tightly focusing the pump beam inside the active medium, it is possible to achieve a high population inversion density at the centre of the laser beam, leaving the beam edges without gain. One can then expect the effective saturation power in the active medium to be lower than in the case where the population inversion is homogeneous across the laser beam [13,23,24].

2.2 Translation of the focusing lens

To investigate this external control, we use the short cavity configuration of Figure 1b. M_2 (transmission $T_2 = 1\%$ at 1 064 nm) is a spherical mirror of 200-mm radius of curvature. The saturable absorber is a 1-mm long antireflection coated Cr^{4+}:YAG plate whose small-signal intensity transmission at 1 064 nm is 85%. The cavity length is reduced to 27 mm and the saturable absorber is placed against the active medium. In this case, the laser mode radius w_G is experimentally measured to be 120 μm. In order to change the pump mode radius w_P in the active medium, the pump beam (150 μm fibre core diameter) is first collimated by the lens L_1 (microscope objective with 10× magnification) and then focused in the active medium by the lens L_2 (microscope objective with 63× magnification). In a first step, the pump mode radius in the active medium is set at 270 μm, *i.e.*, larger than the laser mode waist. In this case, the pulse full-width at half-maximum is 18 ns and the repetition rate is 2 kHz for a pump power of 800 mW. It oscillates in a single longitudinal mode and its average output power is measured to be 0.6 mW. Integration of equations (1) using the experimental parameters for this cavity (see Tab. 1) yields the results shown in Figure 3a. When $1/R = 12.5$, a train of pulses is obtained at a repetition rate of 2 kHz, with a pulse duration of 11 ns, close to the experimental value. It is then predicted that, by varying $1/R$ from 12.5 to 40, the pulse duration increases from 11 ns to 310 ns, and the repetition rate increases from 2 kHz to 70 kHz.

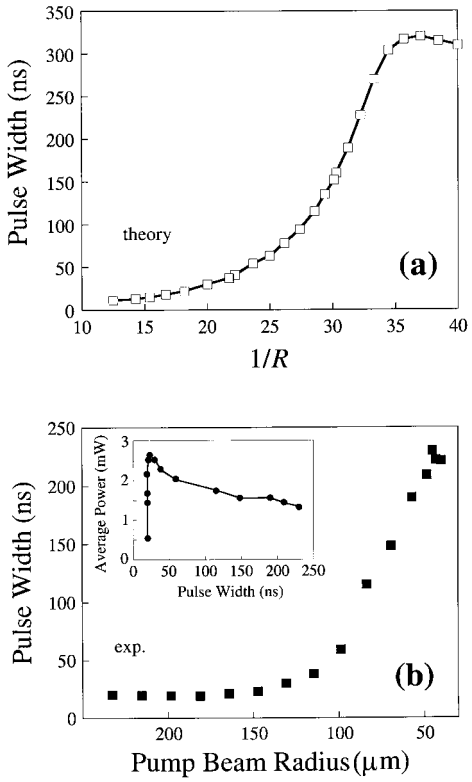

Fig. 3. Results obtained by translation of the focusing lens. (a) Theoretical pulse width *versus* $1/R$. (b) Measured pulse width *versus* pump beam radius. Inset: measured average output power *versus* pulse width.

To obtain experimentally the corresponding variation of the saturation powers ratio, we simply change w_P by moving the position of L_2 along the laser axis up to the position where the pump beam focus matches the laser medium position. Due to the focusing of the pump beam after L_2 (about 15°), we observe that the pump-mode radius is decreased from 270 μm to 40 μm. This tighter focusing of the pump beam increases the pulse width from 18 ns to 240 ns, as shown in Figure 3b. At the same time, the repetition rate increases from 2 kHz to 67 kHz and the average power of the laser decreases to 1.3 mW for long pulses, as shown in the inset of Figure 3b. These experimental observations show that a variation of the pump mode in the active medium indeed changes the saturation power of the laser mode in the active medium. Note that here the variations of R may not be directly related to the ratio w_P/w_G. However, this simple model correctly predicts the tendencies followed by the pulse parameters. Namely, it yields correct values for the pulse lengths, including the presence of the experimentally observed extremum. The similarity between the model and the experimental values confirms that the external focusing of the pump beam gives access to the saturation power ratio governing the Q-switching dynamics.

We have thus shown theoretically and experimentally in this section two techniques, an internal one and an external one, to control the pulse duration by one order of magnitude. In both cases, it is also shown that we can obtain longer pulse durations at the expense of a loss in the average output power. Indeed, as R is decreased (slow Q-switching regime), (i) more gain is wasted to saturate the absorber, leading to a lower peak power, and (ii) the population inversion at the end of the pulse is higher, leading to a higher repetition rate. As a result, the overall efficiency is decreased. In the following section, we focus on a laser geometry where we wish to control accurately the powers circulating in the active medium and in the absorber, in an attempt to maintain a high power efficiency. This leads us to a two-axis laser cavity, as is now described.

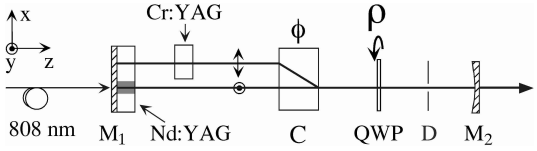

Fig. 4. Experimental arrangement of the forked eigenstate laser: Nd:YAG, active medium; Cr:YAG, saturable absorber; M_1, plane mirror; M_2, concave mirror; C, birefringent crystal; ϕ, phase retardance of C; QWP, quarter-wave plate; ρ, angle between the fast axis of QWP and the x-axis; D, diaphragm.

3 Forked-eigenstate laser

The so-called forked eigenstate consists in a laser mode which is simultaneously oscillating on several parallel beams [14,15]. A two-axis configuration suggests that, if the active medium and the saturable absorber are placed in the two different arms, one can control the relative amounts of power of the mode in the active medium and in the absorber. The model used in the preceding section has to be extended however, in order to take the two-axis geometry into account. To this aim, we use the spatially generalized Jones matrix analysis [14].

3.1 Theoretical model

Consider the laser cavity of Figure 4. Its propagation axis is z. It is closed by two mirrors M_1 and M_2 and contains an isotropic active medium. A birefringent crystal C cut at 45° of its optical axis is inserted inside the cavity. This birefringent element (retardance ϕ) separates spatially the ordinary (y) and the extraordinary (x) polarizations inside the cavity. The polarization walk-off which separates the two beams between M_1 and C is $\Delta x = 1$ mm. The two eigenaxes are superimposed between C and the output coupler, as warranted by the diaphragm D. The saturable absorber is inserted in the extraordinary arm only. The laser is pumped by a fiber-coupled laser diode emitting at 808 nm. The end of the fiber is simply butted against the active medium in the region of the ordinary arm. To impose the forked-eigenstate oscillation, *i.e.*, one mode oscillating simultaneously in the two arms, we insert the quarter-wave plate QWP inside the cavity.

This quarter-wave plate can be rotated around the z-axis with an angle ρ between its fast axis and the x-axis. Depending on the orientation of this plate, the powers circulating in the two separated arms of the laser may change.

3.1.1 Calculation of the cold-cavity eigenstates

In view of calculating these powers, let us recall that, in a two-propagation-axis laser, one must use 4×4 generalized Jones matrices to take into account the transverse shift between the ordinary and extraordinary beams [14,15]. In order to derive first the stationary eigenstates of such a laser, one has to solve the following eigenproblem:

$$\mathbf{M}_4\mathbf{E}_1 = \lambda\mathbf{E}_1, \tag{3}$$

where $\mathbf{M}_4$ is the overall Jones matrix for one round trip inside the cavity starting from M_1,

$$\mathbf{E}_1 = \begin{bmatrix} E_{Tx} \\ E_{Ty} \\ E_{Bx} \\ E_{By} \end{bmatrix} \tag{4}$$

is the electromagnetic field four-component eigenvector on M_1 and λ is the associated eigenvalue. The two upper terms of these vectors correspond to the x- and y-polarized components of the electromagnetic field propagating in the extraordinary arm (top arm), and the two lower terms correspond to the x- and y-polarized components of the electromagnetic field propagating in the ordinary arm (bottom arm). The 4×4-Jones matrix $\mathbf{M}_4$ is given by:

$$\mathbf{M}_4 = \mathbf{GBAG}, \tag{5}$$

where $\mathbf{A}$ and $\mathbf{B}$ are the 4×4-Jones matrices for the forward and backward one-way propagation inside the cavity, respectively, and $\mathbf{G}$ holds for the gain and absorption media:

$$\mathbf{G} = \begin{bmatrix} t_\mathrm{a} & 0 & 0 & 0 \\ 0 & t_\mathrm{a} & 0 & 0 \\ 0 & 0 & t_\mathrm{g} & 0 \\ 0 & 0 & 0 & t_\mathrm{g} \end{bmatrix}. \tag{6}$$

With the same notations as in equations (1), the gain and absorption transmission coefficients t_g and t_a read:

$$t_\mathrm{g} = \exp\left[\frac{L}{2c}\kappa(n_\mathrm{u} - n_\mathrm{d})\right], \tag{7}$$

$$t_\mathrm{a} = \exp\left\{-\frac{L}{2c}\left[a + (a_0 - a)\frac{\sigma_\mathrm{ESA}}{\sigma_\mathrm{GSA}}\right]\right\}. \tag{8}$$

The matrices $\mathbf{A}$ and $\mathbf{B}$ are given by:

$$\mathbf{A} = \sqrt{R_1}\exp(\mathrm{i}kL)\sqrt{T}\,\mathbf{D}\,\mathbf{L}(\rho)\mathbf{C}_+, \tag{9}$$

$$\mathbf{B} = \sqrt{R_2}\exp(\mathrm{i}kL)\sqrt{T}\,\mathbf{C}_-\,\mathbf{L}(\rho)\mathbf{D}, \tag{10}$$

where R_1 and R_2 are the intensity reflection coefficients of mirrors M_1 and M_2, respectively, and T holds for the intracavity losses. The generalized Jones matrices of the intracavity birefringent crystal for the $+z$ and $-z$ directions are given by:

$$\mathbf{C}_+ = \begin{bmatrix} 0 & 0 & 0 & 0 \\ 0 & \mathrm{e}^{-\mathrm{i}\phi/2} & 0 & 0 \\ \mathrm{e}^{\mathrm{i}\phi/2} & 0 & 0 & 0 \\ 0 & 0 & 0 & \mathrm{e}^{-\mathrm{i}\phi/2} \end{bmatrix} \tag{11}$$

and

$$\mathbf{C}_- = \begin{bmatrix} 0 & 0 & \mathrm{e}^{\mathrm{i}\phi/2} & 0 \\ 0 & \mathrm{e}^{-\mathrm{i}\phi/2} & 0 & 0 \\ 0 & 0 & 0 & 0 \\ 0 & 0 & 0 & \mathrm{e}^{-\mathrm{i}\phi/2} \end{bmatrix}, \tag{12}$$

respectively, where ϕ is the retardance introduced by the birefringent crystal. The generalized Jones matrices for the intracavity aperture and the quarter-wave plate are respectively given by:

$$\mathbf{D} = \begin{bmatrix} 0 & 0 & 0 & 0 \\ 0 & 0 & 0 & 0 \\ 0 & 0 & 1 & 0 \\ 0 & 0 & 0 & 1 \end{bmatrix} \tag{13}$$

and

$$\mathbf{L}(\rho) = \begin{bmatrix} \ell(\rho) & 0\;0 \\ 0\;0 & 0\;0 \\ 0\;0 & \ell(\rho) \end{bmatrix}, \tag{14}$$

where the usual 2×2-Jones matrix of the quarter-wave plate is:

$$\ell(\rho) = \begin{bmatrix} \cos^2\rho\,\mathrm{e}^{\mathrm{i}\pi/4} + \sin^2\rho\,\mathrm{e}^{-\mathrm{i}\pi/4} & \mathrm{i}\sqrt{2}\sin\rho\cos\rho \\ \mathrm{i}\sqrt{2}\sin\rho\cos\rho & \sin^2\rho\,\mathrm{e}^{\mathrm{i}\pi/4} + \cos^2\rho\,\mathrm{e}^{-\mathrm{i}\pi/4} \end{bmatrix}. \tag{15}$$

We then calculate the matrix $\mathbf{M}_4$ to be:

$$\mathbf{M}_4 = K\begin{bmatrix} \cos(2\rho)t_\mathrm{a}^2\mathrm{e}^{\mathrm{i}\phi} & 0\;0 & \sin(2\rho)t_\mathrm{a}t_\mathrm{g} \\ 0 & 0\;0 & 0 \\ 0 & 0\;0 & 0 \\ \sin(2\rho)t_\mathrm{a}t_\mathrm{g} & 0\;0 & -\cos(2\rho)t_\mathrm{g}^2\mathrm{e}^{-\mathrm{i}\phi} \end{bmatrix}, \tag{16}$$

where K is a complex constant containing propagation factors common to both arms. By solving equation (3) using equation (16), one obtains the self-consistent eigenvectors $\mathbf{E}_1$. By using the upper and lower components, it follows that the top and bottom powers are finally:

$$I_T = |E_{Tx}|^2 + |E_{Ty}|^2 \tag{17a}$$

$$I_B = |E_{Bx}|^2 + |E_{By}|^2. \tag{17b}$$

It appears here that the powers travelling in both arms are expected to be dependent on ρ. In order to illustrate this behavior in a simple way, let us derive the powers in the two arms when (i) there is no gain nor absorption ($t_g = t_a = 1$) and (ii) C induces no phase shift ($\phi = 0$). In this case, resolution of equation (3) using equation (16) yields the simple normalized eigenvectors:

$$\mathbf{E}_1^+ = \begin{bmatrix} \sin\rho \\ 0 \\ 0 \\ \cos\rho \end{bmatrix}, \tag{18a}$$

$$\mathbf{E}_1^- = \begin{bmatrix} \cos\rho \\ 0 \\ 0 \\ -\sin\rho \end{bmatrix}. \tag{18b}$$

Hence, two orthogonal forked eigenstates are found. Indeed, their amplitudes have non vanishing components in both arms of the laser. In this case, the normalized powers read $I_{T1} = \sin^2\rho$ and $I_{B1} = \cos^2\rho$ for the first forked eigenstate, and $I_{T2} = \cos^2\rho$ and $I_{B2} = \sin^2\rho$ for the second forked eigenstate. From this cold-cavity analysis, we can draw the following conclusions: (i) the powers circulating in the two arms of the laser depend strongly on the rotation angle ρ of the quarter-wave plate, (ii) by pumping only the bottom arm of the laser, only one eigenstate is expected to oscillate (the one for which $I_B/I_T > 1$), (iii) by placing the absorber on the other arm of the laser, the oscillating forked eigenstates will have an adjustable distribution of powers in the gain medium and in the absorber. We hence expect this cavity to provide an accurate control of the laser dynamics.

3.1.2 Derivation of the rate equations for the two-axis laser

In order to predict the dynamical behavior of the laser, one has now to take into account the temporal variations of the powers, which were calculated in the stationary state above. These variations lead to variations of the coefficients of $\mathbf{G}$ and of the generalized Jones matrix for the whole cavity. Thus, the time varying self-consistent condition becomes:

$$\mathbf{E}_1\left(t + \frac{2L}{c}\right) = \mathbf{M}_4\mathbf{E}_1(t). \tag{19}$$

Alternatively, we choose in the following to consider the intracavity electromagnetic field $\mathbf{E}_2$ on mirror M_2, *i.e.*, at the laser output. This field is governed by:

$$\mathbf{E}_2\left(t + \frac{2L}{c}\right) = \mathbf{M}_4'\mathbf{E}_2(t), \tag{20}$$

where $\mathbf{M}_4' = \mathbf{A}\mathbf{G}^2\mathbf{B}$ is the generalized Jones matrix for one round trip inside the cavity starting from the output mirror. The Jones 4-vector $\mathbf{E}_2$ of the intracavity field on mirror M_2 is given by:

$$\mathbf{E}_2 = \begin{bmatrix} 0 \\ 0 \\ E_x\exp(\mathrm{i}\varphi_x) \\ E_y\exp(\mathrm{i}\varphi_y) \end{bmatrix}. \tag{21}$$

Note that, owing to the aperture D, the laser intracavity field on the output mirror M_2 may be represented by the usual Jones 2-vector:

$$\mathbf{E} = \begin{bmatrix} E_x\exp(\mathrm{i}\varphi_x) \\ E_y\exp(\mathrm{i}\varphi_y) \end{bmatrix}. \tag{22}$$

Finally, we use a first-order approximation to write the electromagnetic field after one round trip inside the cavity as:

$$\mathbf{E}\left(t + \frac{2L}{c}\right) = \mathbf{E}(t) + \frac{2L}{c}\frac{\mathrm{d}\mathbf{E}(t)}{\mathrm{d}t}. \tag{23}$$

Then the differential equations of evolution of the laser read:

$$\frac{\mathrm{d}E_x}{\mathrm{d}t} = \frac{c}{2L}\mathrm{Re}\left\{\exp(-\mathrm{i}\varphi_x)[(\mathbf{M}_2(t) - \mathbf{1})\mathbf{E}]\cdot\hat{\mathbf{x}}\right\}, \tag{24a}$$

$$\frac{\mathrm{d}\varphi_x}{\mathrm{d}t} = \frac{c}{2L}\frac{1}{E_x}\mathrm{Im}\{\exp(-\mathrm{i}\varphi_x)[(\mathbf{M}_2(t) - \mathbf{1})\mathbf{E}]\cdot\hat{\mathbf{x}}\}, \tag{24b}$$

$$\frac{\mathrm{d}E_y}{\mathrm{d}t} = \frac{c}{2L}\mathrm{Re}\{\exp(-\mathrm{i}\varphi_y)[(\mathbf{M}_2(t) - \mathbf{1})\mathbf{E}]\cdot\hat{\mathbf{y}}\}, \tag{24c}$$

$$\frac{\mathrm{d}\varphi_y}{\mathrm{d}t} = \frac{c}{2L}\frac{1}{E_y}\mathrm{Im}\{\exp(-\mathrm{i}\varphi_y)[(\mathbf{M}_2(t) - \mathbf{1})\mathbf{E}]\cdot\hat{\mathbf{y}}\}, \tag{24d}$$

$$\frac{\mathrm{d}n_u}{\mathrm{d}t} = \gamma_u(P - n_u) - \zeta(n_u - n_d)I_T(t) - \zeta n_u\varepsilon, \tag{24e}$$

$$\frac{\mathrm{d}n_d}{\mathrm{d}t} = \gamma_u n_u - \gamma_d n_d + \zeta(n_u - n_d)I_T(t) + \zeta n_u\varepsilon, \tag{24f}$$

$$\frac{\mathrm{d}a}{\mathrm{d}t} = \gamma_a(a_0 - a) - \mu a\, I_B(t), \tag{24g}$$

where $\mathbf{M}_2$ is the 2×2 lower right submatrix of $\mathbf{M}_4'$. I_T and I_B are given in equations (17), in which E_{Tx}, E_{Ty}, E_{Bx}, and E_{By} are derived from $\mathbf{E}_1(t) = \mathbf{G}\mathbf{B}\mathbf{E}_2(t)$. The laser dynamics can be obtained by numerical integration of equations (24) by using a fourth-order Runge-Kutta algorithm [22]. The parameters of simulation are shown in the last column of Table 1.

First, we find theoretically that this laser can indeed emit a train of Q-switched pulses. A pulse shape is depicted in Figure 5 when $\rho = 27.5°$. It can be seen that the phases in the top and bottom arms of the fork vary during the emission of pulses. This shows that a description based on a time-varying self-consistent condition is necessary. However, the small phase difference observed means that the polarization of the two-axis laser pulse remains almost linear. Figure 5 also shows that the ratio of the powers in the top and bottom arms of the laser is almost constant during the pulse emission. Moreover, the model predicts that the Q-switched pulse width and repetition rate varies with ρ. Indeed, when $\rho = 45°$, the powers are expected to be almost identical in the two arms and,

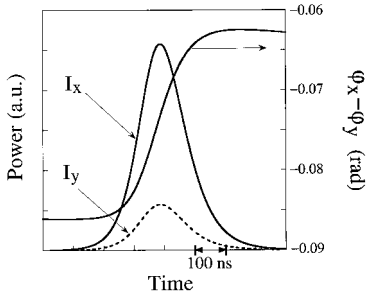

Fig. 5. Theoretical pulse shapes of the x- and y-polarized components of the mode power on the output mirror M_2, together with the phase difference $\varphi_x - \varphi_y$ *versus* time when $\rho = 27.5°$.

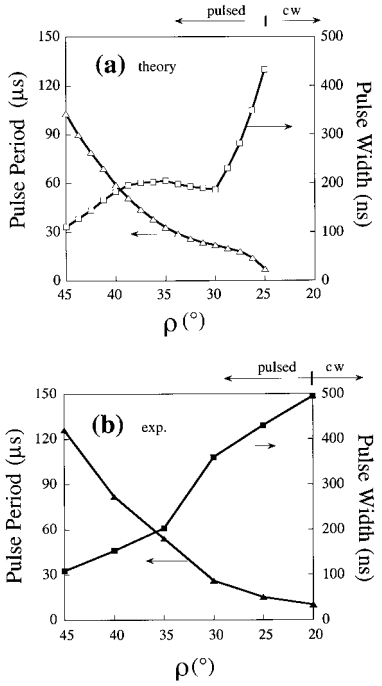

Fig. 6. (a) Simulation results: squares, pulse width *versus* ρ; triangles, pulse period *versus* ρ. The laser operates in the Q-switched regime when $\rho \geq 25°$ and in the cw regime when $\rho < 25°$. (b) Corresponding experimental results. The laser operates in pulsed regime when $\rho \geq 20°$ and in cw regime when $\rho < 20°$.

with the parameter values given in Table 1, the model predicts a full-width at half-maximum of 110 ns for the pulses. If now ρ is decreased, we expect the top power I_T to decrease, and hence the pulse width to lengthen (slow Q-switching regime). The simulation indeed predicts that the pulse width is stretched from 110 ns to 430 ns when ρ is decreased from 45° to 25° [see Fig. 6a]. When ρ is further decreased from 25° to 0°, the laser is expected to operate in the cw regime, since the power circulating in the absorber arm is not high enough to bleach its losses (at $\rho = 0°$, $I_T = 0$). The Q-switch second threshold is thus predicted to be obtained at $\rho = 25°$. In addition, we obtain from the simulation that, when the pulse width is lengthened, the repetition rate increases from 10 kHz to 142 kHz [pulse period decreases from 100 μs to 7 μs, as depicted in Fig. 6a]. This is explained by the fact that the forked eigenstate benefits from a higher gain when ρ is low. On the contrary, when $\rho = 45°$, it experiences the lowest gain, hence the highest threshold, yielding the lowest repetition rate.

3.2 Experimental results

To check these predictions experimentally, we use the scheme depicted in Figure 4. The active medium is a 1.1-mm long crystal of 1 at.% doped Nd:YAG. The 90-mm-long resonator is closed by a plane mirror M_1, coated on the active medium, and a 200-mm radius of curvature concave mirror M_2, with transmission $T_2 = 1\%$ at 1 064 nm, which serves as the output coupler. C is a birefringent YVO_4 crystal, cut at 45° to its optical axis. Both faces of this crystal are antireflection coated at 1 064 nm. The saturable absorber is a [001]-cut Cr:YAG crystal. To avoid nonlinear losses due to the anisotropic saturation of the absorbing ions [25,26], the [100] axis of this crystal is aligned with x. The absorber small-signal intensity transmission at 1 064 nm is 90%. We introduce a quarter-wave plate with anti-reflection coatings on both faces. When we rotate this phase plate from $\rho = 45°$ to $\rho = 20°$, we observe that the pulse width is stretched from 109 ns to 495 ns, and that the repetition rate increases from 8 kHz to 100 kHz [pulse period decreases from 125 μs to 10 μs, as depicted in Fig. 6b]. In this whole range, the laser oscillates in a single longitudinal mode. The "second threshold" is then witnessed between 25° and 20°, after which the laser operates in the cw regime ($20° < \rho < 0°$). These results, reproduced in Figure 6b, are in fairly good agreement with the simulation. The discrepancy between the theoretical and experimental values on the second threshold angle is attributed to the fact that the non-saturable losses are not kept perfectly constant when the quarter-wave plate is rotated (about 15% variation). Moreover, it is worth noting that, even if this pulse stretching is accompanied by a decrease of the peak power [see Fig. 7a], the average output power increases monotonously [see Fig. 7b]. Indeed, in the forked-eigenstate regime, the overall gain of the eigenstate is higher for low values of ρ. Conversely, at $\rho = 45°$, approximately half of the forked-eigenstate power propagates inside the gain medium, leading to a lower average output power. These results are opposite to the ones obtained in single-axis cavity schemes.

4 Discussion and conclusion

We have shown that, provided a solid-state laser with a given saturable absorber, it is possible to control the emitted pulse length either by changing the focusing conditions in the active media (gain and absorber) or using forked eigenstates. All these methods rely on the interplay of the saturation powers in the active media during the pulse build-up: when the saturation power of the absorber is raised and/or the saturation power of the population inversion is lowered, then the pulses are lengthened

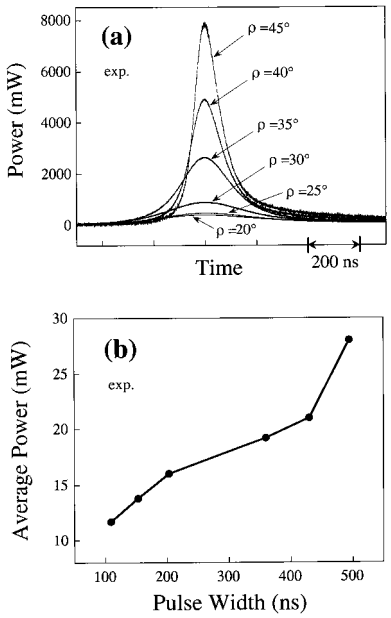

Fig. 7. (a) Experimental recordings of six different pulses for values of ρ from 45° to 20°. The pulse width increases from 109 ns up to 495 ns while the peak power varies from 7 950 mW down to 400 mW. (b) Experimental average output power *versus* pulse width.

and the repetition rate increases. This is obtained in the three cavity configurations. Among these, the translation of the absorber inside the cavity seems the simplest procedure. However, when microchip lasers are considered, the method based on changing the pump focusing inside the gain medium gives probably the only possible solution to adjust the pulse length. Moreover, this method also applies to short cavity designs as, *e.g.*, two-frequency lasers for the generation of high-frequency beat notes [26]. But, as in the first case, the average power decreases when the pulses are lengthened. On the contrary, our forked-eigenstate laser gives not only the opportunity to turn the fixed absorber into an adjustable one, but also to have higher average powers for longer pulses. Furthermore, the physics of the two-axis forked-eigenstate laser permits to cross the Q-switching second threshold, having the ability with a unique cavity geometry to go from cw operation down to a 100 ns pulse regime, by a simple rotation of the quarter-wave plate. In agreement with the model, we hence observe that this forked-eigenstate laser acts as a laser with an adjustable saturable absorber. Besides this original physical insight on Q-switching dynamics, this may find new applications.

In conclusion, we have demonstrated novel methods to control the pulses in passively Q-switched solid-state lasers. The pulse width is easily variable in the 20 ns to 500 ns range. Simulations using a rate-equations model give a good agreement with the experiments performed on Nd:YAG–Cr:YAG diode pumped lasers.

We thank G. Lemasson and Y. Denimal for their early interest in this work, D. Dolfi and L. Morvan for fruitful discussions, and J. Marty and L. Fulbert for their help. This work was partially supported by the Délégation Générale de l'Armement, the Action Concertée Incitative Photonique, and by the Conseil Régional de Bretagne in the framework of the Centre Laser et Applications à la Chimie et aux Télécommunications.

References

1. S. Li, S. Zhou, P. Wang, Y.C. Chen, K.K. Lee, Opt. Lett. **18**, 203 (1993).
2. U. Keller, K.J. Weingarten, F.X. Kärtner, D. Kopf, B. Braun, I.D. Jung, R. Fluck, C. Hönninger, N. Matuschek, J. Aus der Au, IEEE J. Sel. Top. Quant. Electron. **2**, 435 (1996).
3. J.J. Zayhowski, Rev. Laser Engineer. **26**, 841 (1998).
4. H.J. Eichler, A. Haase, M.R. Kokta, R. Menzel, Appl. Phys. B **58**, 409 (1994).
5. P. Yankov, J. Phys. D: Appl. Phys. **27**, 1118 (1994).
6. Y. Shimony, Z. Burshtein, A. Ben-Amar Baranga, Y. Kalisky, M. Strauss, IEEE J. Quant. Electron. **QE-32**, 305 (1996).
7. A. Agnesi, S. Dell'Acqua, G.C. Reali, Opt. Commun. **133**, 211 (1997).
8. G.H.C. New, T.B. O'Hare, Phys. Lett. A **68**, 27 (1978); A.E. Siegman, *Lasers* (University Science Books, Mill Valley, CA, 1986).
9. J.E. Midwinter, Brit. J. Appl. Phys. **16**, 1125 (1965).
10. W.E. Schmid, IEEE J. Quant. Electron. **QE-16**, 790 (1980) and references therein.
11. J.J. Degnan, IEEE J. Quant. Electron. **QE-31**, 1890 (1995).
12. X. Zhang, S. Zhao, Q. Wang, Q. Zhang, L. Sun, S. Zhang, IEEE J. Quant. Electron. **QE-33**, 2286 (1997).
13. X. Zhang, S. Zhao, Q. Wang, B. Ozygus, H. Weber, J. Opt. Soc. Am. B **17**, 1166 (2000).
14. F. Bretenaker, A. Le Floch, J. Opt. Soc. Am. B **8**, 230 (1991).
15. M. Brunel, A. Le Floch, F. Bretenaker, J. Marty, E. Molva, Appl. Opt. **37**, 2402 (1998).
16. A. Szabo, R.A. Stein, J. Appl. Phys. **36**, 1562 (1965).
17. M. Michon, IEEE J. Quant. Electron. **QE-2**, 612 (1966).
18. F.E. Hovis, M. Stuff, C.J. Kennedy, B. Vivian, IEEE J. Quant. Electron. **QE-28**, 39 (1992).
19. M. Hercher, Appl. Opt. **6**, 947 (1967).
20. G. Xiao, J.H. Lim, S. Yang, E. van Stryland, M. Bass, L. Weichman, IEEE J. Quant. Electron. **QE-35**, 1086 (1999).
21. A. Suda, A. Kadoi, K. Nagasaka, H. Tashiro, K. Midorikawa, IEEE J. Quant. Electron. **QE-35**, 1548 (1999).
22. W.H. Press, S.A. Teukolsky, W.T. Wetterling, B.P. Flannery, *Numerical Recipes in Fortran 90* (Cambridge University Press, Cambridge, UK, 1996).
23. D.G. Hall, R.J. Smith, R.R. Rice, Appl. Opt. **19**, 3041 (1980).
24. G. Martel, C. Ozkül, F. Sanchez, Opt. Commun. **185**, 419 (2000).
25. N.N. Ilichev, A.V. Kir'yanov, E.S. Gulyamova, P.P. Pashinin, Quant. Electron. **28**, 17 (1998) [Kvant. Elektron. **25**, 19 (1998)].
26. M. Brunel, O. Emile, M. Vallet, F. Bretenaker, A. Le Floch, L. Fulbert, J. Marty, B. Ferrand, E. Molva, Phys. Rev. A **60**, 4052 (1999).